Atmospheric
Chemistry
and Physics

Variability of NO$_x$ in the polar middle atmosphere from October 2003 to March 2004: vertical transport vs. local production by energetic particles

M. Sinnhuber[1], B. Funke[2], T. von Clarmann[1], M. Lopez-Puertas[2], G. P. Stiller[1], and A. Seppälä[3]

[1]Karlsruhe Institute of Technology, Institute for Meteorology and Climate Research, Karlsruhe, Germany
[2]Instituto de Astrofìsica de Andalucìa, CSIC, Granada, Spain
[3]Finish Meteorological Institute FMI, Helsinki, Finland

Correspondence to: M. Sinnhuber (miriam.sinnhuber@kit.edu)

Abstract. We use NO, NO$_2$ and CO from MIPAS/ENVISAT to investigate the impact of energetic particle precipitation onto the NO$_x$ budget from the stratosphere to the lower mesosphere in the period from October 2003 to March 2004, a time of high solar and geomagnetic activity. We find that in the winter hemisphere the indirect effect of auroral electron precipitation due to downwelling of upper mesospheric/lower thermospheric air into the stratosphere prevails. Its effect exceeds even the direct impact of the very large solar proton event in October/November 2003 by nearly 1 order of magnitude. Correlations of NO$_x$ and CO show that the unprecedented high NO$_x$ values observed in the Northern Hemisphere lower mesosphere and upper stratosphere in late January and early February are fully consistent with transport from the upper mesosphere/lower thermosphere and subsequent mixing at lower altitudes. In the polar summer Southern Hemisphere, we observed an enhanced variability of NO and NO$_2$ on days with enhanced geomagnetic activity, but this seems to indicate enhanced instrument noise rather than a direct increase due to electron precipitation. A direct effect of electron precipitation onto NO$_x$ can not be ruled out, but, if any, it is lower than 3 ppbv in the altitude range 40–56 km and lower than 6 ppbv in the altitude range 56–64 km. An additional significant source of NO$_x$ due to local production by precipitating electrons below 70 km exceeding several parts per billion as discussed in previous publications appears unlikely.

1 Introduction

Energetic particle precipitation has been acknowledged as a source of large disturbances to the chemical composition mainly of the polar middle atmosphere for several decades. Already in the 1970s, it was recognized by Crutzen et al. (1975) and Porter et al. (1976) that precipitating energetic particles can be a source of NO$_x$ (N, NO, NO$_2$) in the middle atmosphere, as a result of excitation, decomposition, and ionization of the most abundant species, and due to subsequent chemical reactions of positive ions with neutral species. Shortly afterwards, it was recognized that positive ion chemistry will also release active hydrogen HO$_x$ (H, OH, HO$_2$) from its source, H$_2$O (Solomon et al., 1981). As both HO$_x$ and NO$_x$ destroy ozone in catalytic cycles – HO$_x$ roughly above 45 km, NO$_x$ below 45 km (Lary, 1997) – energetic particle precipitation events are also precursors of ozone loss in the middle atmosphere.

HO$_x$ is very short-lived throughout the middle atmosphere, and HO$_x$ budgets will recover quickly after atmospheric ionization events. However, NO$_x$ can be quite long-lived, depending on solar illumination – the photochemical lifetime varies from hours in the sunlit middle mesosphere to days in the sunlit middle stratosphere and weeks in polar night. Thus, during polar winter, NO$_x$ produced by energetic particle precipitation can be transported down from its source regions in the polar mesosphere or lower thermosphere into the polar stratosphere, where it will then contribute to stratospheric ozone loss. This is called the "EPP indirect effect" as opposed to the "EPP direct effect" due to local production in

the stratosphere and lower mesosphere (Randall et al., 2007). The impact of solar proton events is nowadays reasonably well understood, in part thanks to the series of very large solar proton events during the maximum of solar cycle 23 (Jackman et al., 2001, 2005; Funke et al., 2011; Rohen et al., 2005). There is also evidence of a large indirect effect of energetic electron precipitation for many polar winters now (Randall et al., 2006, 2009; Funke et al., 2005a).

While effects due to large solar proton events and the indirect electron effects are reasonably well established, it is to date not clear whether there is a direct impact of energetic electron precipitation onto the stratosphere and lower mesosphere. The observational evidence gathered so far appears to be ambiguous. Callis et al. (1998) have argued for a large impact of energetic electrons onto the stratosphere based on model calculations. However, no observational evidence of a direct impact below 80 km is provided by these authors. Large NO$_x$ productions due to geomagnetic activity or relativistic electrons from the magnetosphere have been reported by Renard et al. (2006) for January 2004 and by Clilverd et al. (2009) for 11–15 February 2004. However, both observations are ambiguous. Seppälä et al. (2007) discuss both events but interpret the first as a result of transport from the auroral zone, the second event in February as local production of NO$_x$. Hauchcorne et al. (2007) also show NO$_2$ increases in mid-January 2004 and argue that those are consistent with downward transport after the sudden stratospheric warming in December rather than with local production. Similar results are obtained in a model study considering a strong auroral NO$_x$ source in mid-winter 2003/2004 (Semeniuk and McConnell, 2005). Funke et al. (2007) argue that the observations of January 2004 reported by Renard et al. (2006) are equally consistent with downward transport of NO$_x$ from the lower thermosphere, and that is more likely than direct production. Observations of MIPAS (Fischer et al., 2008) on ENVISAT considering both NO$_x$ and the dynamical tracer CH$_4$ suggest that the very strong NO$_x$ enhancement reported by Clilverd et al. (2009) in February 2004 is also more likely due to downwelling (Lopez-Puertas et al., 2006). Evidence of a possible strong impact of relativistic electrons from the radiation belt on ozone in the middle stratosphere during mid-winter is reported by Sinnhuber et al. (2006). However, the linking mechanism from radiation belt electrons to stratospheric ozone is not clear, as no NO$_x$ measurements or other more direct evidence of an impact of electron precipitation at these altitudes has been presented. Verronen et al. (2011) have shown a direct impact of energetic electron precipitation on the OH abundance above 70 km altitude during two large geomagnetic storms in March 2005 and April 2006, with smaller contributions down to 50 km during one event. Sinnhuber et al. (2011) have used a long-term data set of NO$_x$ measurements (NO+NO$_2$) from HALOE/UARS from 1991 to 2005 to investigate the direct impact of energetic electron precipitation onto the middle atmosphere. Their study also shows a direct contribution from

electrons mainly above 80 km, with smaller and rather sporadic contributions to lower altitudes. However, due to the poor horizontal coverage of HALOE, the results at altitudes below 80 km are not really robust. Thus it is not clear yet how large the direct impact of energetic electron precipitation on altitudes below 80 km to the overall NO$_x$ budget is.

A more detailed summary of energetic particle precipitation onto atmospheric composition and their long-term consequences is given in the recent review by Sinnhuber et al. (2012).

We use observations of NO and NO$_2$ from the MIPAS instrument onboard the ENVISAT satellite for the geomagnetically very active period from October 2003 to end of March 2004 to investigate the possible direct impact of energetic particle precipitation onto NO$_x$ in the middle atmosphere below 70 km. CO, a tracer for air from the upper mesosphere or thermosphere and for downward transport, is used to distinguish between the direct and indirect impact during polar winter.

In Sect. 2, the MIPAS data used are presented. In Sect. 3, the geomagnetic and solar activity as well as the dynamical condition of the period analyzed is discussed. In Sect. 4.1, observations in the winter hemisphere and, in Sect. 4.2, observations in the summer hemisphere are discussed.

2 MIPAS data

The Michelson Interferometer for Passive Atmospheric Sounding (MIPAS) was a mid-infrared Fourier transform spectrometer observing a large number of atmospheric trace gases in limb-sounding observation mode (Fischer et al., 2008). MIPAS was launched as one of three atmospheric missions on the European Environmental Satellite ENVISAT on 1 March 2002, and operated until the loss of ENVISAT in April 2012. ENVISAT was in a sun-synchronous orbit with an Equator crossing time of 10:00 a.m. local solar time in descending mode. In 2002–2004, MIPAS sampled the atmosphere horizontally with a latitudinal spacing of $\approx 5°$ in latitude. As MIPAS measurements require no sunlight, 28 measurements are obtained in each latitude bin every day, providing a very good horizontal coverage. In the nominal measurement mode used in this study, MIPAS scans the limb tangentially from about 6 up to 68 km.

We use NO, NO$_2$ and CO from MIPAS calibration version V3O derived with the level-2 IMK/IAA research processor (von Clarmann et al., 2003). Only data from version 14 are used for NO, versions 14 and 15 for NO$_2$, and versions 12 and 13 for CO. As NO2_14 and NO2_15 are very similar, as well as CO_12 and CO_13, this provides a stable, self-consistent data set. Vertical resolution is 4–8 km for NO and NO$_2$ and 6–12 km for CO in the altitude range of 20–70 km. More details about MIPAS NO and NO$_2$ can be found, e.g., in Funke et al. (2005b, 2011), and about CO in Funke et al. (2009).

Where daily averages have been used, NO, NO$_2$ and CO data with low sensitivity have been excluded by applying a threshold to the mean value of the averaging kernel (AK) matrix (Rodgers, 2000) diagonal element. The AK diagonal elements represent a measure of the sensitivity of the retrieval at a given profile grid point to the true volume mixing ratio (VMR). Values close to zero (here ≤ 0.03) indicate that there is no significant sensitivity to the abundance at the corresponding altitude. All daily averages are calculated as area weighted values.

NO mixing ratio increases strongly from the lower mesosphere to the lower thermosphere. Thus observations at mesospheric tangent altitudes have a strong thermospheric NO signal in the line of sight, which might provide an additional positive offset of up to 1.5 ppbv, henceforth called "thermospheric cross-talk". For the retrieval of NO$_2$ no such information crosstalk happens because the concentration of NO$_2$ decreases strongly from the upper stratosphere to the thermosphere even during nighttime. Thus the measured signal is dominated by radiance emitted near the tangent altitude of each limb observation. Therefore, in the winter hemisphere where NO$_x$ values are on the order of tens of parts per billion to thousands of parts per billion by volume, observations of NO$_x$ (NO+NO$_2$) are used, while in the summer hemisphere, where mixing ratios might be in the range of below 1 ppbv, nighttime NO$_2$ and daytime NO are treated separately.

3 Northern winter 2003–2004: solar activity, geomagnetic activity, and vortex dynamics

3.1 Solar and geomagnetic activity

The time period from first of October 2003 to end of March 2004 was chosen because it was, on the one hand, a period of very high geomagnetic activity, and, on the other hand, it contained one of the largest solar particle events directly observed by particle detectors from space so far. In Fig. 1 different proxies for energetic particle precipitation for this time are shown: the Ap index as an indicator of geomagnetic activity; a merged data set of electron fluxes from the POES instrument combining two upward-looking channels to derive 100–300 keV precipitating electrons as described in Sinnhuber et al. (2011); and proton fluxes as measured in geostationary orbit by the particle counters onboard GOES-10. Both Ap index and proton fluxes are available online from the National Geophysical Data Center (NGDC; spidr.ngdc.noaa.gov/spidr).

Geomagnetic activity is high throughout the observation period, with several very pronounced intervals of enhanced geomagnetic activity lasting for many days: in mid-October 2003 before the solar proton event, in mid-November 2003, in mid-December 2003, in late January 2004, in mid-February 2004, and in mid-March 2004. These are accom-
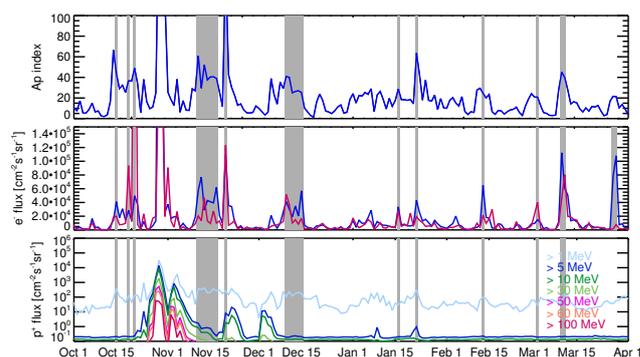

Figure 1. Proxies for energetic particle precipitation into the atmosphere from 1 October 2003 to 30 March 2004. Top: the global Ap index as a proxy for geomagnetic activity. Middle: 100–300 keV electrons measured by the POES SEM/SEM-2 sensors in the 0° channel, which looks upward in polar regions. Red: Northern Hemisphere, blue: Southern Hemisphere. Bottom: proton fluxes at different energies measured by particle sensors on the GOES-10 satellite. Marked in grey are periods of enhanced electron fluxes (see text).

panied by high fluxes of energetic electrons, especially large during several sporadic events lasting only several hours – e.g., on 15, 19, and 21 October 2003; on 11–17 and 20 November 2003; on 10–15 December 2003; on 16 and 22 January 2004; on 13 February 2004; and 2, 10, 11 and 27/28 March 2004 (marked in grey in Fig. 1). Highest electron fluxes are observed during 29 October–1 November, at the period of the solar proton event. However, during this period the electron channels of the POES instruments are likely contaminated by high-energy protons. Solar proton events are clearly detected by enhanced proton fluxes over a large energy range from 1 to 100 MeV, with ≤ 10 MeV protons exceeding fluxes of 1 proton cm^{-2} s^{-1} sr^{-1} from 26 October to 7 November 2003. Two smaller solar proton events occur around 20–23 November and in early December 2003. During these events, proton fluxes were several orders of magnitude lower than for the October/November events, and did not exceed 10 protons cm^{-2} s^{-1} sr^{-1} for either the ≤ 10 MeV protons – which affect altitudes down to the lower mesosphere – or the ≤ 30 MeV protons – which affect altitudes down to the upper stratosphere.

3.2 Vortex dynamics

Additionally to the high geomagnetic activity, the polar winter Northern Hemisphere 2003/2004 was characterized by an interesting dynamical condition, with the occurrence of a major stratospheric warming and a vortex breakup in the upper stratosphere in late December, followed by a re-forming of the polar vortex in late January, and very strong descent which lasted well into March 2004 (Funke et al., 2009; Manney et al., 2005) accompanied by high planetary wave activity both before and after the sudden stratospheric warming (Pancheva et al., 2008). A more detailed view of this
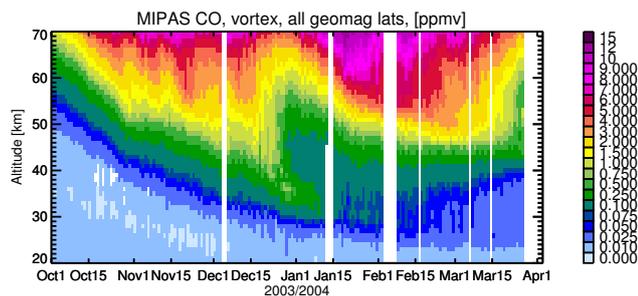
Figure 2. CO as measured by MIPAS in the Northern Hemisphere from October 2003 to March 2004 in the latitude bin from 40 to 90° N, considering both day and night observations. All geomagnetic latitudes but only within the polar vortex (equivalent latitudes (Butchart and Remsberg, 1986) polewards of 65°). Only days with more than eight data points were used.

winter is provided by observations of the temporal evolution of CO inside the polar vortex as shown in Fig. 2. Due to its strong vertical gradient and longevity in the polar winter vortex, carbon monoxide is commonly used as a tracer of air originating from the upper mesosphere and lower thermosphere, which is transported down into the lower mesosphere and stratosphere in the polar vortex. Enhanced values of CO are observed already in early October 2003 above 50 km, progressing steadily downward to ≈ 40 km until late October, signifying that a stable vortex has already formed. During November and December, downwelling of CO-rich air continues, but not as steadily as in early October, presumably due to the already enhanced wave activity that finally led to the sudden stratospheric warming event and vortex breakup in late December. Enhanced CO VMRs reach about 30 km altitude in early December. In late December, the sudden stratospheric warming event starts in the upper stratosphere and mesosphere, leading to a vortex breakup there. CO mixing ratios between 40 and 60 km altitude decrease very quickly due to mixing with mid-latitude air. Above 60 km, CO mixing ratios also decrease, but slower than in the upper stratosphere. Below 40 km, the vortex persists until January, and downwelling of CO is observed until mid-January in this altitude region. In the mesosphere above 60 km, CO mixing ratios increase again in early January, and CO-rich air progresses downward steadily until late January, signifying the re-formation of the polar vortex and continuing downwelling in the mesosphere. However, in February and March, CO values first level off and then decrease due to the increasing contribution of photochemical loss after polar sunrise. Thus, after late January CO is not a perfect quantitative indicator of downwelling in the polar vortex, but it can still be used for identification of dynamical short-term variability in a qualitative sense.

4   Results

4.1   NO$_x$ in the Northern Hemisphere polar vortex

The temporal evolution of NO$_x$ (NO+NO$_2$) inside the polar vortex in Northern Hemisphere winter 2003/2004 is shown in the upper panel of Fig. 3. Three contour lines of CO are shown as well for a direct comparison between NO$_x$ and CO (see also Fig. 2). The solar proton event on 30 October–1 November 2003 is clearly visible as a strong increase of about 1 order of magnitude of NO$_x$ values within 1 day in the altitude range 40–70 km. Above about 60 km altitude, NO$_x$ is already enhanced several days before the onset of the solar proton event. This might be due to downwelling in the polar vortex in early October as observed in CO observations at the same time. After the solar proton event, the behavior of NO$_x$ closely resembles the behavior of CO as shown both in Fig. 2 and by the CO isolines in Fig. 3: downwelling of enhanced NO$_x$ values in the upper stratosphere and lower mesosphere continues until the major stratospheric warming in late December, when NO$_x$ values below 60 km altitude decrease very quickly. Above 60 km, high values of NO$_x$ continue even after the major warming. From mid-January on, downwelling of air very rich in NO$_x$ is observed again, in agreement with GOMOS observations at latitudes north of 80° (see Hauchcorne et al., 2007). Unlike CO, stratospheric NO$_x$ mixing ratios do not level off in late January and February, but persist to propagate downward very steadily with an average speed of ≈ 400 m/day from the mid-mesosphere around 66 km in late January down to 45 km in mid-March (see Fig. 4). Stratospheric NO$_x$ enhancements persist after March 2004 until at least July as shown in Randall et al. (2005). In the stratosphere, the lifetime of NO$_x$ is on the order of days to weeks even in the sunlit atmosphere (see, e.g., Friederich et al., 2013). In the lower mesosphere above 55 km altitude, NO$_x$ decreases during February because the NO$_x$ lifetime is on the order of few days after polar sunrise. While during the two periods of downwelling in October–mid-December and January–March CO mixing ratios are similar and reach values of 10–15 ppmv above 60 km altitude in both periods, NO$_x$ mixing ratios are quite different before and after the stratospheric warming event. During the strong downwelling in January and February 2004, observed NO$_x$ mixing ratios are more than 1 order of magnitude higher than those produced during the solar proton event inside the polar vortex, reaching values of more than 1000 ppbv in the daily average in late January and early February, compared to more than 100 ppbv directly after the solar proton event.
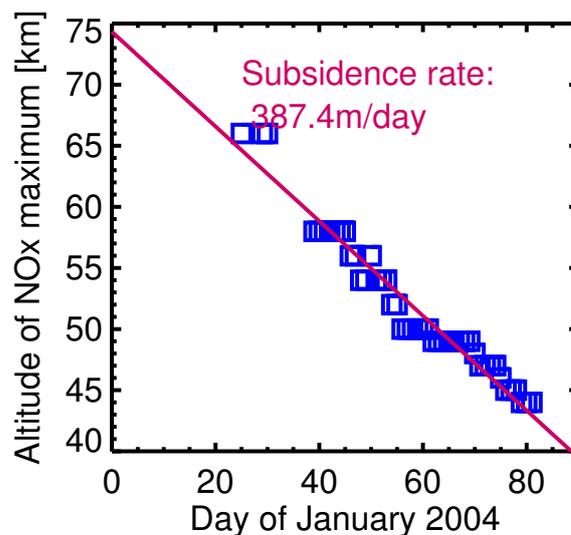
NO$_x$ mixing ratios of more than 1000 ppbv first appear in mid-January at altitudes above 65 km, and NO$_x$-rich air proceeds steadily downward in the following weeks. In the following, it will be assessed whether these high amounts of NO$_x$ are produced locally during the period of the strong geomagnetic activity in mid-January, or are due to downwelling of air from the NO maximum in the auroral zone
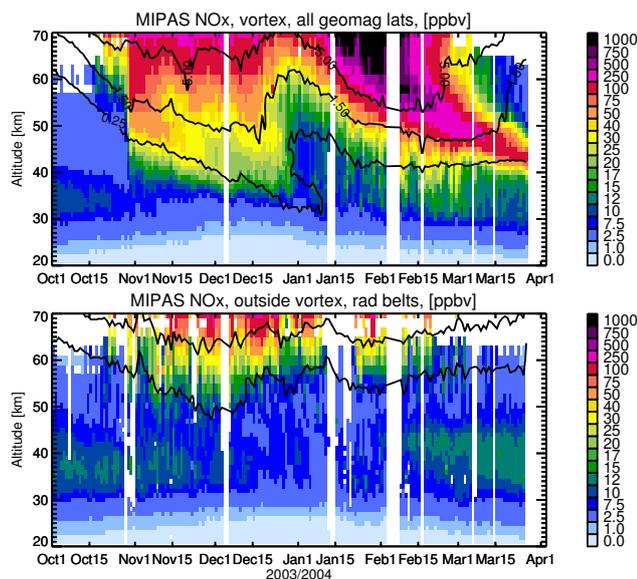
Figure 3. Top panel: as Fig. 2, but for NO$_x$ (NO+NO$_2$). Lower panel: as upper panel, but outside the polar vortex (equivalent latitudes $\leq 55°$), and sampled only in the radiation belt region (geomagnetic latitudes of 55–68°). Bold lines are CO isolines of 0.25, 1.5 and 5.0 ppmv sampled in the same way as indicators of vertical transport and vortex origin.


Figure 4. Blue squares: temporal evolution of the peak altitude of NO$_x$ as observed in MIPAS observations inside the polar vortex (equivalent latitudes polewards of 65° N), from January through March 2004. The red line is the result of a least-square fit to those observations, giving an average subsidence rate of 400 m day^{-1} for the NO$_x$ maximum.
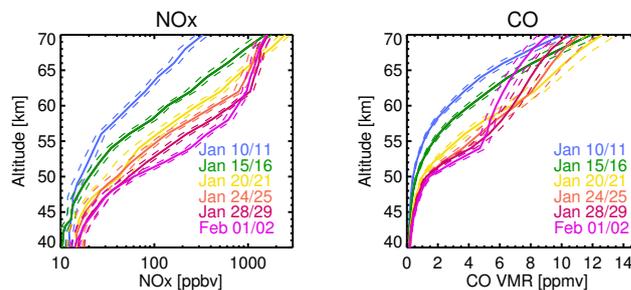
Figure 5. Two-daily average altitude profiles of NO$_x$ (left) and CO (right) on six 2-day periods from 10 January 2004 to 2 February 2004, inside the polar vortex (equivalent latitudes poleward of 65°). Dashed lines denote the error of the mean.

($\approx$ 90–120 km). Figure 5 shows daily averaged NO$_x$ and CO altitude profiles inside the polar vortex for 6 days from 10 January to 2 February. Both NO$_x$ and CO show a consistent behavior during this time period: an increase of the mixing ratios from 10 to 20 January at all altitudes, and the development of a "knee" due to photochemical loss, which is more pronounced at higher altitudes, after 20 January. The increase in VMR appears to be consistent with downwelling for both gases. The increase in NO$_x$ VMRs at a given altitude is stronger than the increase in CO, because the volume mixing ratio of NO$_x$ increases exponentially with altitude, the VMR of CO, linearly. Photochemical loss becomes evident for both NO$_x$ and CO between 20 and 24 January, but for CO it covers a larger vertical range: the "knee" is observed at 54 km on 2 February for CO, compared to 60–62 km for NO$_x$ on the same day.

CO is relatively stable in the polar winter vortex; the only processes acting on local CO abundances are downward transport, mixing, and photochemical loss due to the reaction with OH. Photochemical loss of NO$_x$ occurs with a different rate and over a different altitude regime as seen before. However, transport and mixing will act on NO$_x$ in the same way as on CO, so the temporal evolution of the relationship between NO$_x$ and CO can provide evidence of a direct local production of NO$_x$ in the altitude range observed by the MIPAS data, i.e., below about 70 km. A compact, non-linear relationship exists between NO$_x$ and CO until 19 January (see left panel of Fig. 6). Non-linearity results

from the different vertical gradients of NO$_x$ and CO as seen in Fig. 5. The upper branch of the relationship with CO values $\geq$ 10 ppmv and NO$_x$ values $\geq$ 700 ppbv appears only after 14 January, at altitudes above 60 km. Maximal values of more than 12 ppmv CO and more than 2000 ppbv NO$_x$ are reached on 18/19 January. The increase of both NO$_x$ and CO at the same time suggests downwelling of air from the upper mesosphere/lower thermosphere as a source. As maximum values of NO$_x$ are reached on 18/19 January, their source can therefore not be direct production during the strong geomagnetic storm of 22 January as suggested, e.g., by Renard et al. (2006).

In the left panel of Fig. 6, the secant to the NO$_x$–CO relationship is marked as a dashed line. The region comprised by this secant and the NO$_x$–CO distribution (grey area) can
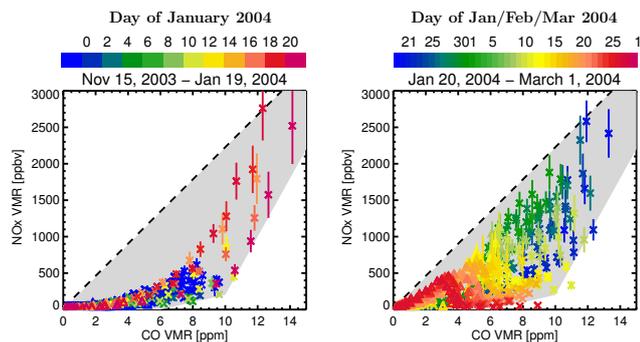
Figure 6. Scatterplot of NO$_x$ and CO as observed by MIPAS within the polar vortex throughout NH winter 2003–2004. Left: from 15 November 2003 to 19 January 2004, considering observations in the altitude range 40–70 km. The symbols are color-coded by time, with blue denoting days in 2003, and the days in January 2004 running from green–yellow–orange–red. Dark red is 19 January. The dashed line marks the secant to this distribution; light grey marks the region incorporated by the observed distribution and its secant. Right: from 20 January to 1 March 2004. Grey area and dashed line as in left panel. Colors mark the day, running from dark blue–green–yellow–orange–red. Error bars show the error of the mean of the daily averages of NO$_x$.

be filled in by mixing processes. Photochemical loss of NO$_x$ would move the NO$_x$–CO pairs down, while photochemical loss of CO would move NO$_x$–CO pairs to the left. Values above this region can be gained by direct local production of NO$_x$, e.g., due to energetic particle precipitation, or by photochemical loss of CO. In the first days after 20 January 2004, the grey mixing region is indeed filled in, while later (mid- to late February), the NO$_x$–CO pairs are moved to the left and downward. This indicates that, during the time interval from 20 January 2004 to 1 March 2004, both mixing processes and photochemical loss of NO$_x$ and CO are important. As discussed before, from mid-February on, a knee develops in NO$_x$ due to the different photochemical loss rates of NO$_x$ and CO in the upper stratosphere and lower mesosphere. This is observed as a local NO$_x$ maximum at moderately high CO values in the right panel of Fig. 6. Values above the mixing secant are not observed, so there is no evidence of a direct local production of NO$_x$ below 70 km during this time from these observations.

In particular, there is no evidence of a strong increase of NO$_x$ in the altitude range 50–70 km during mid-February, as discussed in Clilverd et al. (2009) based on GOMOS observations. To investigate this in more detail, NO$_x$ values sampled only within the geomagnetic latitudes corresponding to the radiation belts are shown in the lower panel of Fig. 3. To further exclude masking of local production by the large background values within the polar vortex, only values well outside the polar vortex (equivalent latitudes $\leq 55°$) are considered. Enhanced values of NO$_x$ are observed above 50–60 km altitude continuously from end of October 2003

to mid-February 2004. However, they are closely enveloped by isolines of enhanced CO values, and they thus are more likely remnants of vortex air than resulting from direct NO$_x$ production. This close relationship between enhanced values of NO$_x$ and CO throughout mid-February is also seen when looking at the spatial distribution of single observations (see Fig. 7). However, the polar vortex as indicated by high values of both NO$_x$ and CO is elongated at the beginning of this period indicating a wave 2 pattern as discussed, e.g., in Pancheva et al. (2008). This pattern moves and expands to a more circular form from 8 to 15 February. Because of the wave 2 pattern, the vortex edge is shifted far to the north on 8/9 February, and GOMOS observations poleward of 70° are taken partly outside the polar vortex (see Fig. 8). In Fig. 8, a comparison of nighttime NO$_2$ between single-point observations of MIPAS and GOMOS is shown 6 days between late January and mid-February. GOMOS observations both inside and outside the polar vortex agree very well with neighboring MIPAS data points, but significantly higher values are also observed by MIPAS further in the vortex core. On 14/15 February, GOMOS observations poleward of 70° are obtained all inside the polar vortex. They are significantly higher than the neighboring MIPAS observations, though well within the range of MIPAS data elsewhere in the vortex. The reason for the apparent disagreement between daily averages of NO$_2$ from MIPAS and GOMOS in this time period thus appears to be the strongly elongated vortex as well as an inhomogeneous distribution of NO$_x$ inside the vortex. This inhomogeneous distribution is already apparent and observed by both instruments in late January; see left panel of Fig. 8.

Apart from the solar proton event in October/November 2003, no indication of direct NO$_x$ production is observed in the MIPAS data in the Northern Hemisphere winter at altitudes below 70 km either inside or outside the polar vortex. Thus, a strong increase of NO$_x$ due to local production by energetic electron precipitation below 70 km, as discussed, e.g., by Clilverd et al. (2009), appears highly unlikely during this winter. However, it is still possible that smaller direct local NO$_x$ production due to energetic particles occur, but they are masked by the very high values observed in NO$_x$ especially in late January and February 2004. This can thus be better investigated by studying the summer hemisphere, where downwelling from the upper mesosphere or lower thermosphere does not play a role. This will be investigated in more detail in the next section.

4.2 Southern Hemisphere summer

In the Southern Hemisphere, it is polar summer in the time period investigated. Background values of NO$_x$ are therefore low in the upper stratosphere and lower mesosphere, and small changes can then be better discerned than in the Northern Hemisphere winter. However, this requires very precise observations. Because of this, NO and NO$_2$ will be
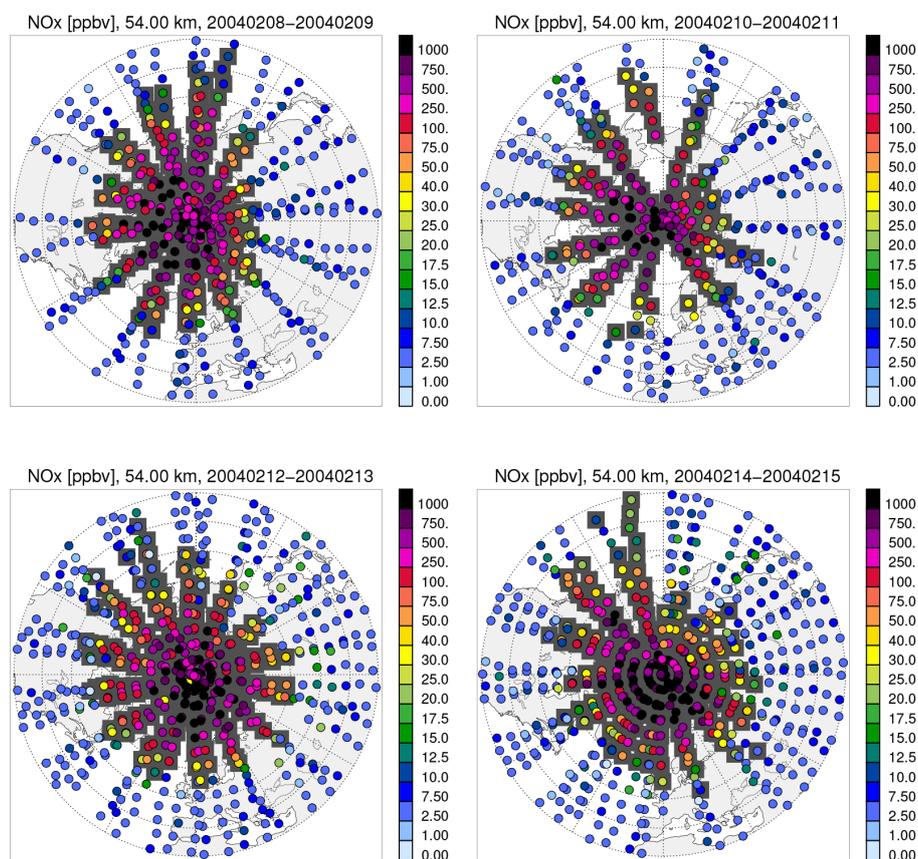
Figure 7. NO$_x$ (day and night) single observations from MIPAS at 54 km altitude from 8 to 16 February 2004. Grey rectangles mark observations where the corresponding CO value was larger than 1 ppmv marking, e.g., observations within the vortex.
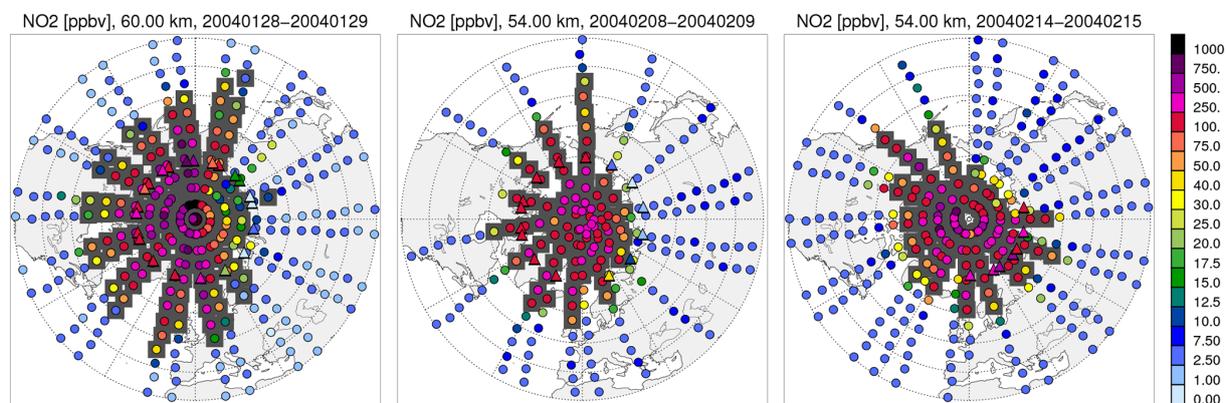
Figure 8. MIPAS (circles) and GOMOS (triangles) single observations of nighttime NO$_2$ at solar zenith angles $\geq 106°$. Left: 60 km, 28–29 January 2004; middle: 54 km, 8–9 February 2004; right: 14–15 February 2004. Grey rectangles as in Fig. 7.
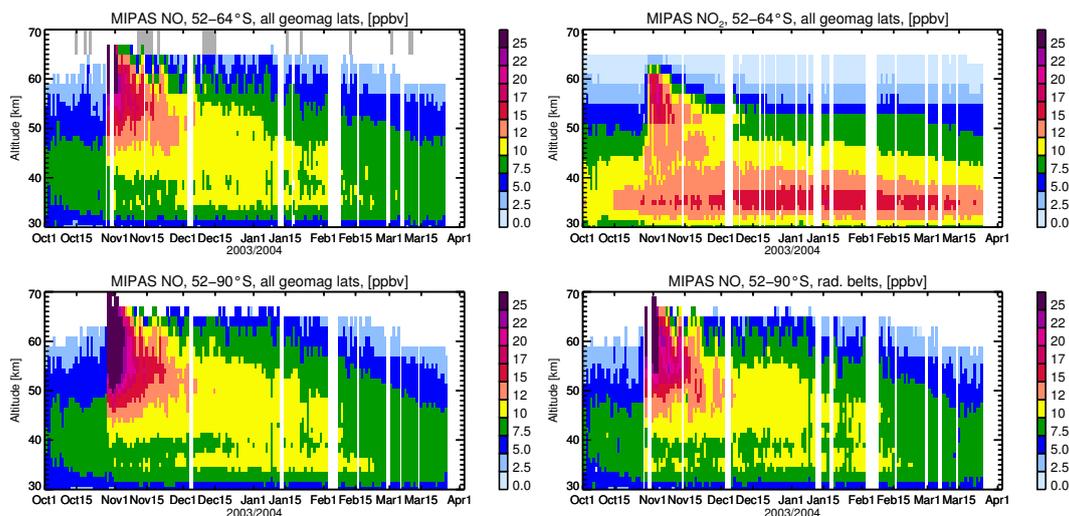
Figure 9. Temporal evolution of daytime NO (solar zenith angle, SZA, $\leq 88°$) and nighttime NO$_2$ (SZA $\geq 98°$) at high southern latitudes from 1 October 2003 to 30 March 2004. Top left: daily averages of NO from 52 to 64° S considering all geomagnetic latitudes. Marked in grey are days of enhanced electron fluxes; see also Fig. 1. Top right: NO$_2$ sampled over the same area. Lower panel: NO sampled over 52–90° S. Left: all geomagnetic latitudes, right: geomagnetic latitudes corresponding to the radiation belts. Only days with more than 15 data points are considered for NO, only days with more than 10 data points for NO$_2$, and only data points within ± 5 median absolute deviations are considered for averaging.

investigated separately in the following, as NO observations in the lower mesosphere are prone to contaminations due to thermospheric cross-talk of up to 1.5 ppbv. Such a cross-talk is not present in NO$_2$ because mesospheric and thermospheric NO$_2$ values are very low. NO values are sampled during daytime at solar zenith angles $\leq 88°$, and NO$_2$ during nighttime at solar zenith angles $\geq 98°$, because the partitioning of NO$_x$ favors NO during daytime, NO$_2$ during nighttime in this altitude range. As it is polar summer, this limits NO$_2$ observations to latitudes equatorwards of 64° S. To limit sampling errors, only days with more than 10 (NO$_2$) and 15 (NO) data points are considered, and only data points within 5 median absolute deviations are considered for the daily averages.

The temporal evolution of NO and NO$_2$ in the latitude range 52–64° S from October 2003 through March 2004 is shown in Fig. 9. NO and NO$_2$ show a distinct annual variability in the upper stratosphere (30–40 km) with maximal values during summer. The most distinct feature is the solar proton event in late October 2003, which leads to an increase of several tens of parts per billion by volume in both NO and NO$_2$ above 35 km within 1 day. As NO$_x$ is photochemically destroyed in the sunlit atmosphere, it then decreases in the following days to weeks, reaching again background values in mid-November around 60 km and in mid-December around 50 km. In the latitude range chosen, 52–64° S, enhanced NO$_x$ values do not decrease steadily. This is due at least partly to the sampling of an inhomogeneous and variable field of high values over a small (latitudinal) area. If the complete polar cap is sampled, enhanced NO$_x$ values decrease more steadily

(exponentially) after the solar proton event, as shown, e.g, in Friederich et al. (2013) for NO$_x$, and in the lower left panel of Fig. 9 for daytime NO.
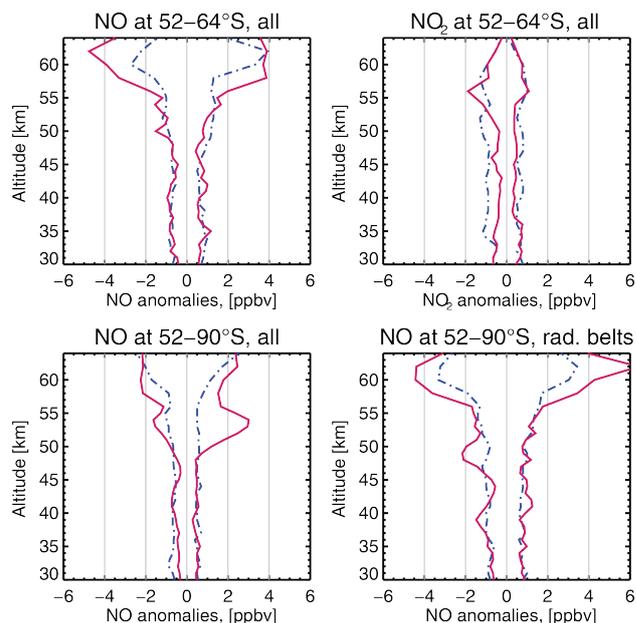
Additionally to the strong enhancement of NO$_x$ after the solar proton event in late October 2003, several enhancements with a much shorter lifetime and much smaller amplitudes are observed in NO, e.g., several days before the large solar proton event on 20 October at 58–64 km, on 13 November at 58–64 km, at 18 and 21 November at 58–62 km (see upper left panel of Fig. 9). All 4 days correspond to times of enhanced geomagnetic activity and increased electron precipitation on this or the previous day; see grey marks in upper left panel and Fig. 1. Apart from the very small increase on 5 December, these are also observed (with varying amplitudes) when sampling over 52–90° S, or sampling only geomagnetic latitudes corresponding to the radiation belts (see lower left and right panels of Fig. 9), so are unlikely to be due to sampling effects. The amplitudes of these enhancements are on the order of several parts per billion by volume, too high to be caused by thermospheric cross-talk. However, similar enhancements are not observed in nighttime NO$_2$ (see upper right panel of Fig. 9). This is probably due to the NO$_x$ partitioning, which favors NO above 58 km even during nighttime.

To investigate whether the observed smaller increases in NO around 58–64 km are really due to NO$_x$ production during energetic electron precipitation events, anomalies of NO and NO$_2$ were calculated in the following way. For altitudes between 30 and 70 km, a 7-day running mean was calculated from the daily averages of NO$_2$ and NO (see Fig. 9) as shown
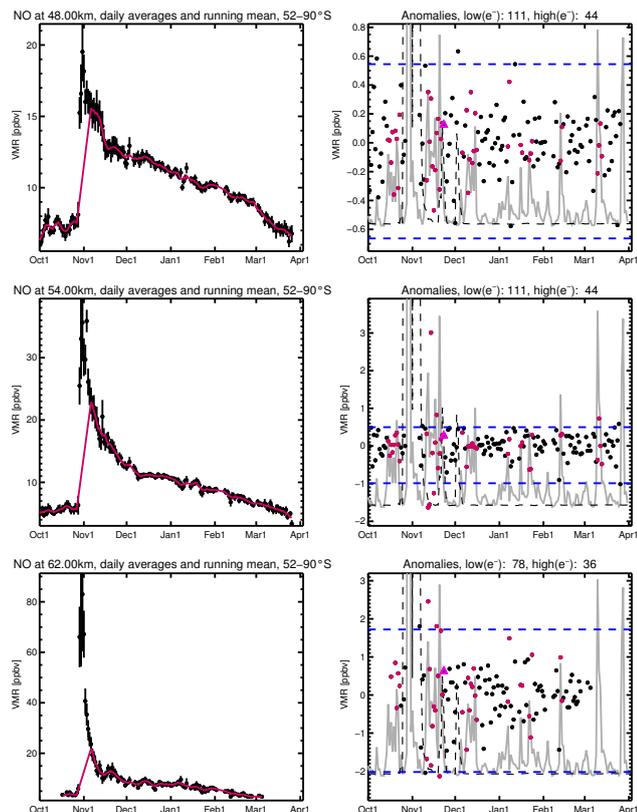
Figure 10. Daytime NO in the latitude region 52–90° S at three altitudes: 48 km (upper panel), 54 km (middle panel), and 62 km (lower panel). Left panels: daily averages (black dots) and 7-day running mean (red line) excluding the period of largest proton forcing from 27 October to 6 November 2003. Right panels: anomalies (dots, daily average – running mean). Days with enhanced electron fluxes ($\geq 2 \times 10^4$ electrons cm^{-2} s^{-1} sr^{-1}) of the 100–300 keV channel on this or the previous day are marked in red. Light grey lines show the 100–300 keV electron fluxes, dashed black lines the ≥ 10 MeV proton flux for reference, both in arbitrary normalized units. Dashed blue lines mark the 1 and 99 % percentile of the anomalies, excluding days with enhanced electron fluxes. The violet triangle marks a day with enhanced electron fluxes and ≥ 10 MeV proton fluxes.

Figure 11. Comparison of 98 % significance level for days with low electron fluxes (blue dashed lines, $\leq 2 \times 10^4$ electrons cm^{-2} s^{-1} sr^{-1} of the 100–300 keV precipitating electrons) with maximal and minimal anomalies of NO$_2$ and NO (red lines) on days of enhanced electron fluxes ($\geq 2 \times 10^4$ electrons cm^{-2} s^{-1} sr^{-1} of the 100–300 keV precipitating electrons) as a function of altitude. Upper left: daytime NO at 52–64° S, all geomagnetic latitudes. Upper right: nighttime NO$_2$ sampled over the same area. Lower left: daytime NO at 52–90° S, all geomagnetic latitudes, and lower right: daytime NO at 52–90° S, geomagnetic latitudes corresponding to the radiation belts (55–68°). The period of largest proton forcing (27 October–6 November) is excluded.

exemplarily in the left panels of Fig. 10. Days with enhanced proton fluxes (≥ 1 proton cm^{-2} s^{-1} sr^{-1} of the ≥ 30 MeV protons) were excluded. This corresponds to the time of the largest proton forcing during 27 October to 6 November. The weaker events in late November and early December were not excluded as proton fluxes were 3–4 orders of magnitude lower than during the October/November events. It should be noted, however, that enhanced electron fluxes and enhanced proton fluxes do not occur on the same days during these events with the exception of 22 November, when the 100–300 keV electron flux is $\geq 2 \times 10^4$ electrons cm^{-2} s^{-1} sr^{-1}, and the 10 MeV proton flux is ≥ 2.8 protons cm^{-2} s^{-1} sr^{-1}. Anomalies are calculated as the difference of the daily average and the 7-day running mean as shown exemplarily

in the right-hand panels of Fig. 10. Days with fluxes of $\geq 2 \times 10^4$ electrons cm^{-2} s^{-1} sr^{-1} of the 100–300 keV precipitating electrons are marked in red. Those days are called "disturbed" in the following. The dashed blue line shows the 1 and 99 % percentile of the distribution of anomalies, considering only days with low electron fluxes (e.g., 100–300 keV electron flux $\leq 2 \times 10^4$ electrons cm^{-2} s^{-1} sr^{-1}), derived from integration of the distribution. Positive anomalies above the 99 % percentile of the "undisturbed" days are observed on several days both at 54 km and at 60 km. However, negative anomalies below the 1 % percentile also occur during "disturbed" days, suggesting that the enhanced values observed on "disturbed" days are more likely due to enhanced instrument noise rather than to an atmospheric response. Results of these investigations are summarized in Fig. 11. Shown are the 1 and 99 % percentile of the distribution of anomalies, considering only "undisturbed" days, compared to the highest and lowest anomalies of the "disturbed" days for altitudes from 30 to 70 km and for the four scenarios shown in Fig. 9. For NO$_2$, both the 98 % confidence

level and the anomalies on "disturbed" days lie between -2 and 2 ppbv. For NO, the 98 % confidence level lies between -2 and 2 ppbv at altitudes below 56 km, but increases to 2–4 ppbv above depending on sampling. This indicates increased noise at higher altitudes. The maximal anomalies of the "disturbed" days behave in a similar way, increasing with altitude. Values above about 56 km are generally higher than the noise level of the "undisturbed" days, but do not show a preference for positive anomalies. This again suggests enhanced noise rather than an atmospheric response. Exceptions are NO at 62 km in the radiation belt region, where a positive anomaly of ≈ 6 ppbv is observed, and NO at 54–56 km sampled over the whole polar cap, where a positive anomaly of ≈ 3 ppbv is observed. Above ≈ 64 km, no meaningful NO and NO$_2$ data can be obtained for quiescent polar summer conditions when NO$_x$ concentrations are very low. This provides an upper limit for an atmospheric response of NO$_x$ due to energetic electron precipitation: on average, it is smaller than 3 ppbv below 54 km, smaller than 6 ppbv between 54 and 64 km. However, the amplitudes of both the 98 % percentile, and of the maximal anomalies, are dominated by the period from 7 to 21 November. During this period, energetic electron fluxes were exceptionally high especially on 21 November, but there was also still a significant amount of NO$_x$ remnant from the solar proton event. This made the derivation of a background difficult, which possibly contributes to the high observed variability. If this period is excluded from the analysis, results are qualitatively very similar, but the amplitudes are lower, less than 1.5 ppbv below 54 km, and less than 3 ppbv above 54 km.

5   Conclusions

- No evidence of a direct impact of energetic electron precipitation in the altitude range of the MIPAS instrument was found with the exception of the solar proton event in October/November 2003.

- Correlations of NO$_x$ and CO show that the unprecedented high NO$_x$ values observed in the lower mesosphere and upper stratosphere in late January and early February are fully consistent with transport from the upper mesosphere/lower thermosphere, and subsequent mixing and photochemical loss at lower altitudes. An additional source of NO$_x$ due to local production at altitudes below 70 km as discussed in previous publications appears highly unlikely.

- Observations of NO and NO$_2$ anomalies in the Southern Hemisphere summer suggest enhanced instrument noise during some electron events. Maximal anomalies observed give an upper limit of the impact of electron precipitation onto daily averaged NO$_x$ at high latitudes: lower than 3 ppbv in 40–56 km and lower than 6 ppbv in 56–64 km.

References

Butchart, N., and Remsberg, E. E.: The area of the stratospheric polar vortex as a diagnostic for tracer transport on an isentropic surface, J. Atmos. Sci, 43, 1219–1339, 1986.

Callis, L. B., Natarajan, M., Lambeth, J. D., and Baker, D. N.: Solar-atmospheric coupling by electrons (SOLACE) 2. Calculated stratospheric effects of precipitating electrons, 1979–1988, J. Geophys. Res., 103, 28.421–28.438, 1998.

Clilverd, M., Seppälä, A., Rodger, C., Mlynczak, M., and Kozyra, J.: Additional stratospheric NO$_x$ production by relativistic electron precipitation during the 2004 spring NO$_x$ descent event, J. Geophys. Res., 114, A04305, doi:10.1029/2008JA013472, 2009.

Crutzen, P. J., Isaksen, I. S., and Reid, G. C.: Solar proton events: stratospheric sources of nitric oxide, Science, 189, 457–458, 1975.

Fischer, H., Birk, M., Blom, C., Carli, B., Carlotti, M., von Clarmann, T., Delbouille, L., Dudhia, A., Ehhalt, D., Endemann, M., Flaud, J. M., Gessner, R., Kleinert, A., Koopman, R., Langen, J., López-Puertas, M., Mosner, P., Nett, H., Oelhaf, H., Perron, G., Remedios, J., Ridolfi, M., Stiller, G., and Zander, R.: MIPAS: an instrument for atmospheric and climate research, Atmos. Chem. Phys., 8, 2151–2188, doi:10.5194/acp-8-2151-2008, 2008.

Friederich, F., von Clarmann, T., Funke, B., Nieder, H., Orphal, J., Sinnhuber, M., Stiller, G. P., and Wissing, J. M.: Lifetime and production rate of NO$_x$ in the upper stratosphere and lower mesosphere in the polar spring/summer after the solar proton event in October–November 2003, Atmos. Chem. Phys., 13, 2531–2539, doi:10.5194/acp-13-2531-2013, 2013.

Funke, B., Lopez-Puertas, M., Gil-Lopez, S., von Clarmann, T., Stiller, G. P., Fischer, H., and Kellman, S.: Downward transport of upper atmospheric NO$_x$ into the polar stratosphere and lower mesosphere during the Antarctic winter 2003 and Arctic winter 2002/2003, J. Geophys. Res., 112, D24308, doi:10.1029/2005JD006463, 2005a.

Funke, B., Lopez-Puertas, M., von Clarmann, T., Stiller, G. P., Fischer, H., Glatthor, N., Grabowski, U., Höpfner, M., Kellmann, S., Kiefer, M., Linden, A., Mengistu Tsidu, G., Milz, M., Steck, T., and Wang, D. Y.: Retrieval of stratospheric NO$_x$ from 5.3 and 6.2 µm nonlocal thermodynamic equilibrium emissions measured by Michelson Interferometer for Passive Atmospheric Sounding (MIPAS) on Envisat, J. Geophys. Res, 110, D09302, doi:10.1029/2004JD005225, 2005b.

Funke, B., Lopez-Puertas, M., Fischer, H., Stiller, G. P., von Clarmann, T., Wetzel, G., Carli, B., and Belotti, C.: Comment on 'Origin of the January–April 2004 increase in strato-

spheric NO$_2$ observed in Northern polar latitudes' by Jean-Baptiste Renard et al., Geophys. Res. Lett., 34, L07813, doi:10.1029/2006GL027518, 2007.

Funke, B., López-Puertas, M., García-Comas, M., Stiller, G. P., von Clarmann, T., Höpfner, M., Glatthor, N., Grabowski, U., Kell-mann, S., and Linden, A.: Carbon monoxide distributions from the upper troposphere to the mesosphere inferred from 4.7 μm non-local thermal equilibrium emissions measured by MIPAS on Envisat, Atmos. Chem. Phys., 9, 2387–2411, doi:10.5194/acp-9-2387-2009, 2009.

Funke, B., Baumgaertner, A., Calisto, M., Egorova, T., Jackman, C. H., Kieser, J., Krivolutsky, A., López-Puertas, M., Marsh, D. R., Reddmann, T., Rozanov, E., Salmi, S.-M., Sinnhuber, M., Stiller, G. P., Verronen, P. T., Versick, S., von Clarmann, T., Vyushkova, T. Y., Wieters, N., and Wissing, J. M.: Composition changes after the "Halloween" solar proton event: the High Energy Particle Precipitation in the Atmosphere (HEPPA) model versus MI-PAS data intercomparison study, Atmos. Chem. Phys., 11, 9089–9139, doi:10.5194/acp-11-9089-2011, 2011.

Hauchecorne, A., Bertaux, J.-L., Dalaudier, F., Russell III, J. M., Mlynczak, M. G., Kyrölä, E., and Fussen, D.: Large increase of NO$_2$ in the north polar mesosphere in January-February 2004: Evidence of a dynamical origin from GOMS/ENVISAT and SABEER/TIMED data, Geophys. Res. Lett., 34, L03810, doi:10.1029/2006GL027628, 2007.

Horne, R. B., Lam, M. M., and Green, J. C.: Energetic electron precipitation from the outer radiation belt during geomagnetic storms, Geophys. Res. Lett., 36, L19104, doi:10.1029/2009GL040236, 2009.

Jackman, C. H., McPeters, R. D., Labow, G. J., Praderas, C. J., and Fleming, E. L.: Northern hemisphere atmospheric effects due to the July 2000 solar proton events, Geophys. Res. Lett., 28, 2883–2886, 2001.

Jackman, C. H., DeLand, M. T., Labow, G. J., Fleming, E. L., Weisenstein, D. K., Ko, M. K. W., Sinnhuber, M., Anderson, J., and Russell III, J. M.: The influence of the several very large solar proton events in years 2000-2003 on the neutral middle atmosphere, Adv. Space Res., 35, 445–450, 2005.

Jackman, C. H., Marsh, D. R., Vitt, F. M., Garcia, R. R., Randall, C. E., Fleming, E. L., and Frith, S. M.: Long-term middle atmospheric influence of very large solar proton events, J. Geophys. Res., 114, D11304, doi:10.1029/2008JD011415, 2009.

Lary, D. J.: Catalytic destruction of stratospheric ozone, J. Chem. Phys., 102, 21515–21526, 1997.

López-Puertas, M., Funke, B., Gil-López, S., von Clarmann, T., Stiller, G. P., Kellmann, S., Fischer, H., and Jackman, C. H.: Observation of NO$_x$ enhancements and ozone depletion in the Northern and Southern hemispheres after the October-November 2003 solar proton events, J. Geophys. Res., 110, A09S43, doi:10.1029/2005JA011050, 2005.

López-Puertas, M., Funke, B., von Clarmann, T., Fischer, H., and Stiller, G. P.: The stratospheric, mesospheric NOy in the 2002-2004 polar winters as measured by MIPAS/ENVISAT, Space Sci. Rev., 125, 403–416, 2006.

Manney, G. L., Krüger, K., Sabutis, J. L., Sena, S. A., and Pawson, S.: The remarkable 2003–2004 winter and other recent warm winters in the Arctic stratosphere since the late 1990s, J. Geophys. Res., 110, D04107, doi:10.1029/2004JD005367, 2005.

Pancheva, D., Mukhtarov, P., Mitchell, N. J., Smith, A. K., Andonov, B., Singer, W., Hocking, W., Meek, C., Manson, A., and Murayama, Y.: Planetary waves in coupling the stratosphere and mesosphere during the major stratospheric warming in 2003/2004, J. Geophys. Res., 113, D12105, doi:10.1029/2007JD009011, 2005.

Porter, H. S., Jackman, C. H., and Green, A. E. S.: Efficiencies for production of atomic nitrogen and oxygen by relativistic proton impact in air, J. Chem. Phys., 65, 154–167, 1976.

Randall, C. E., Harvey, V. E., Manney, G. L., Orsolini, Y., Codrescu, M., Sioris, C., Brohede, S., Haley, C. S., Gordley, L. L., Zawodny, J. M., and Russell III, J. M.: Stratospheric effects of energetic particle precipitation in 2003–2004, Geophys. Res. Lett., 32, L05802, doi:10.1029/2004GL022003, 2005.

Randall, C. E., Harvey, V. E., Singelton, C. S., Bernath, P. F., Boone, C. D., and Kozyra, J. U.: Enhanced NO$_x$ in 2006 linked to strong upper stratospheric Arctic vortex, Geophys. Res. Lett, 33, L18811, doi:10.1029/2006GL027160, 2006.

Randall, C. E., Harvey, V. L., Singleton, C. S., Bailey, S. M., Bernath, P. F., Codrescu, M., Nakajima, H., and Russell III, J. M.: Energetic particle precipitation effects on the Southern Hemisphere stratosphere in 1992–2005, J. Geophys. Res, 112, D08308, doi: 10.1029/2006JD007696, 2007.

Randall, C. E., Harvey, V. L., Siskind, D. E., France, J., Bernath, P. F., Boone, C. D., and Walker, K. A.: NO$_x$ descent in the Arctic middle atmosphere in early 2009, Geophys. Res. Lett., 36, L18811, doi:10.1029/2009GL039706, 2009.

Renard, J.-B., Blelly, P.-L., Bourgeois, Q., Chartier, M., Goutail, F., and Y. J. Orsolini: Origin of the January-April 2004 increase in stratospheric NO$_2$ observed in the Northern polar latitudes, Geophys. Res. Lett., 33, L11801, doi:10.1029/2005GL025450, 2006.

Rodgers, C. D.: Inverse Method for Atmospheric Sounding: Theory and Practice, Series on Atmospheric, Oceanic and Planetary Physics, Vol. 2, World Scientific, edited by: F. W. Taylor, 2000.

Rohen, G. J., von Savigny, C., Sinnhuber, M., Eichmann, K.-U., Llewellyn, E. J., Kaiser, J. W., Jackman, C. H., Kallenrode, M.-B., Schroeter, J., Bovensmann, H., and Burrows, J. P.: Ozone depletion during the solar proton events of Oct./Nov. 2003 as seen by SCIAMACHY, J. Geophys. Res., 110, A09S39, doi:10.1029/2004JA010984, 2005.

Semeniuk, K. and McConnell, J. C.: Simulation of the October-November 2003 solar proton events inthe CMAM GCM: Comparison with observations, Geophys. Res. Lett., 32, L15S02, doi:10.1029/2005GL022392, 2005.

Seppälä, A., Clilverd, M. A, and Rodger, C. J.: NO$_x$ enhancements in the middle atmosphere during 2003–2004 polar winter: Relative significance of solar proton events and the aurora as a source, J. Geophys. Res., 112, D23303, doi:10.1029/2006JD008326, 2007.

Sinnhuber, M., Kazeminejad, S., and Wissing, J. M.: Interannual variation of NO$_x$ from the lower thermosphere to the upper stratosphere in the years 1991–2005, J. Geophys. Res., 116, A02312, doi:10.1029/2010JA015825, 2011.

Sinnhuber, M., Nieder, H., and Wieters, N.: Energetic particle precipitation and the chemistry of the mesosphere/lower thermosphere, Surv. Geophys., 33, 1281–1334, doi:10.1007/s10712-012-9201-3, 2012.

Sinnhuber, B.-M., von der Gathen, P., Sinnhuber, M., Rex, M., König-Langlo, G., and Oltmans, S. J.: Large decadal scale changes of polar ozone suggest solar influence, Atmos. Chem. Phys., 6, 1835–1841, doi:10.5194/acp-6-1835-2006, 2006.

Solomon, S., Rusch, D. W., Gerard, J.-C., Reid, G. C., and Crutzen, P. J.: The effect of particle precipitation events on th neutral and ion chemistry of the middle atmosphere II: odd hydrogen, Planet. Space Sci., 29, 885–892, 1981.

Verronen, P. T., Rodger, C. J., Clilverd, M. A., and Wang, S.: First evidence of mesospheric hydroxyl response to electron precipitation from the radiation belts, J. Geophys. Res., 116, D07307, doi:10.1029/2010JD014965, 2011.

von Clarmann, T., Glatthor, N., Grabowski, U., Höpfner, M., Kellmann, S., Kiefer, M., Linden, A., Mengistu Tsidu, G., Milz, M., Steck, T., Stiller, G. P., Wang, D. Y., Fischer, H., Funke, B., Gil-Lopez, S., and Lopez-Puertas, M.: Retrieval of temperature and tangent altitude pointing from limb emission spectra recorded from space by the Michelson Interferometer for Passive Atmospheric Sounding (MIPAS), J. Geophys. Res., 108, doi:10.1029/2003JD003602, 2003.